



Spectroscopic dielectric tensor of monoclinic crystals: CdWO₄

G. E. Jellison Jr.,* M. A. McGuire, L. A. Boatner, J. D. Budai, E. D. Specht, and D. J. Singh
Material Science and Technology Division, Oak Ridge National Laboratory, Oak Ridge, TN 37831-6092, USA

(Received 16 August 2011; published 9 November 2011)

Generalized ellipsometry measurements were made using 12 orientations of a monoclinic CdWO₄ crystal. Using these measurements and the associated analytical methods presented here, it is shown that the four independent complex elements of the dielectric tensor can be determined at each wavelength. Below the band edge (~ 4 eV), the dielectric tensor is real, and, therefore, it is possible to uniquely diagonalize the dielectric tensor and determine the birefringence for light passing along the unique axis, but the orientation of the dielectric tensor axes will be a function of wavelength. Above the band edge, unique diagonalization is not possible. The generalized ellipsometric spectra show some symmetry in the cross-polarization coefficients. When the unique axis is perpendicular to the sample surface, the condition $\rho_{ps} = -\rho_{sp}$ is valid. If the unique axis is perpendicular to the plane of incidence, $\rho_{sp} = \rho_{ps} = 0$, and if the unique axis is in the plane of incidence, parallel to the sample surface, then $\rho_{ps} = \rho_{sp} \neq 0$. The combined experimental and analytical methods described here are applicable to the determination of the spectroscopic dielectric tensors of monoclinic crystals in general.

DOI: [10.1103/PhysRevB.84.195439](https://doi.org/10.1103/PhysRevB.84.195439)

PACS number(s): 78.20.Ci, 42.25.Ja, 78.70.Ps, 29.40.Mc

I. INTRODUCTION

The optical functions of a material are essential parameters describing the interaction of the material with light.¹⁻³ These functions are often expressed as the complex dielectric function $\varepsilon = \varepsilon_1 - i\varepsilon_2$, which is the quantity that relates the electric displacement vector to the electric field vector $\mathbf{D} = \kappa_o \boldsymbol{\varepsilon} \mathbf{E}$ in Maxwell's equations (κ_o is the permittivity of free space = 8.85×10^{-12} C²/J-m). For many applications, it is often useful to express ε in terms of the complex refractive index, which is related to the dielectric function $\varepsilon = \tilde{n}^2 = (n - ik)^2$. The quantity n is the refractive index, and k is the extinction coefficient, where the optical absorption coefficient is given by $\alpha = 4\pi k/\lambda$, where λ is the wavelength of light.

Since both the displacement and electric field quantities (\mathbf{D} and \mathbf{E}) are three-element complex vectors, then $\boldsymbol{\varepsilon}$ is, in general, a 3×3 complex tensor. The $\boldsymbol{\varepsilon}$ tensor simplifies to a complex scalar for materials with cubic or isotropic symmetry. Materials with hexagonal, trigonal, or tetragonal symmetry are optically uniaxial materials, requiring a tensor to describe the relationship between \mathbf{D} and \mathbf{E} , but the tensor has only two independent parameters in the principal axis system of the dielectric tensor. These are normally called the ordinary (o) and extraordinary (e) dielectric functions, where $\varepsilon_o = \varepsilon_{11} = \varepsilon_{22}$ and $\varepsilon_e = \varepsilon_{33}$, where the prescription (a,b,c) \rightarrow (1,2,3) is used and the optic axis is aligned along the c -axis of the crystal. Crystals with orthorhombic symmetry are biaxial and require three elements in the complex dielectric tensor, where $\varepsilon_{11} \neq \varepsilon_{22} \neq \varepsilon_{33}$. The principal axes of uniaxial and biaxial crystals with orthorhombic symmetry are determined by the symmetry of the crystal, and the resulting dielectric tensors can be diagonalized. That is, it is possible to find a coordinate system determined by the crystal symmetry such that the dielectric tensor is diagonal with the off-diagonal elements equal to 0. Since this coordinate system is determined by the symmetry of the material, it is not a function of wavelength.¹⁻³

However, monoclinic and triclinic materials are different.^{2,3} Monoclinic materials have one principal axis of the dielectric tensor that is defined by the crystalline symmetry, but there is no crystal symmetry that specifies the other two axes. For this

case, the complex dielectric tensor is given by:

$$\boldsymbol{\varepsilon} = \begin{bmatrix} \varepsilon_{11} & \varepsilon_{12} & 0 \\ \varepsilon_{12} & \varepsilon_{22} & 0 \\ 0 & 0 & \varepsilon_{33} \end{bmatrix}. \quad (1)$$

It is possible to find a coordinate system that will diagonalize a monoclinic dielectric tensor at a specific wavelength if $\boldsymbol{\varepsilon}$ is real, but the axes will now be a function of wavelength. If $\boldsymbol{\varepsilon}$ is complex, then it is not possible to diagonalize $\boldsymbol{\varepsilon}$. Triclinic materials are even more complicated in that there are no principal axes defined by symmetry, and the complex dielectric function tensor has six independent components, and it is not in general diagonalizable.

The method of determination of the complex dielectric function for isotropic materials is well known and is best done using spectroscopic ellipsometry.⁴⁻⁸ Since the dielectric function for an isotropic material is a scalar, any orientation of the material will suffice, and most ellipsometers will be capable of performing the required measurements. The isotropy of the sample means that the plane of incidence defines the geometry of the measurement, and there is no cross polarization. (Cross polarization occurs when incident s - or p -polarized light is transformed by reflection into a mixed polarization state including both s - and p -polarized light.) Determination of the dielectric functions of uniaxial materials is somewhat more difficult, but there are several examples of successful measurements in the literature.⁹⁻¹² The difficulty in such cases occurs because the ellipsometric response is now a function of the orientation of the crystal. If the optic axis is not in the plane of incidence or perpendicular to the plane of incidence, then cross polarization occurs. This measurement requires either multiple measurements using standard ellipsometry or a single measurement of a sample with the optic axis appropriately oriented using generalized ellipsometry. (Generalized ellipsometry measures the cross-polarization terms as well as the standard ellipsometric parameters.) Measurement of the complex dielectric function of biaxial materials can only be done using multiple measurements at different orientations of the crystal.

Given the complexity of the measurement and the required data reduction, there are very few measurements of the optical functions of monoclinic materials in the literature. Using a standard rotating polarizer ellipsometer (RPE), Alonso *et al.*^{13,14} measured the ellipsometric parameters at several orientations of a 3,4,9,10-perylene tetracarboxylic dianhydride (PTCDA) organic crystal. The data were reduced to three complex refractive indices (refractive index and extinction coefficient) and two angles at each wavelength, thus taking into account the monoclinic symmetry of the crystal. Later, Tavazzi *et al.*^{15,16} performed similar measurements on organic monoclinic crystals, including polarization-sensitive optical absorption and reflection. Recently, Schmidt *et al.*^{17–19} performed generalized ellipsometry measurements on a series of nanostructured films, which exhibit structural morphology akin to monoclinic symmetry. To take into account the assumed monoclinic structure of the films, Schmidt *et al.* applied an additional projection operator to transform the system to a nonorthogonal coordinate system.²⁰ The work of Refs. 15–20 reduced the dielectric functions to three complex diagonal components, compared to the four components that are required by group theory.

While it is well understood from a theoretical perspective that monoclinic crystals require four complex elements of the dielectric tensor, often the off-diagonal element is not determined experimentally, particularly for spectroscopic determinations of the dielectric tensor. In this work, we address this issue and show that it is possible to determine all four complex dielectric functions associated with the dielectric tensor for monoclinic materials. We accomplish this by performing a series of 12 generalized ellipsometry measurements on different orientations of a CdWO₄ crystal and by reducing the data using Berreman matrices.²¹ By using this approach, we obtain accurate spectra of the four complex dielectric functions, including the off-diagonal term. We also show that the transform employed by Schmidt *et al.*^{17–19} cannot be used for CdWO₄. In addition, the generalized ellipsometry measurement also measures the cross-polarization components very accurately, enabling us to explore the symmetries of these cross-polarization components as a function of the orientation of the crystal.

II. EXPERIMENT

A. Sample

Generalized ellipsometry measurements were performed on a CdWO₄ single crystal that had been cut into a cube $1 \times 1 \times 1 \text{ cm}^3$. CdWO₄ is a known scintillator material²² with a monoclinic, Wolframite-type structure, and it belongs to the space group $P2/c \equiv C_{2h}$,⁴ number 13 in the *International Tables for X-Ray Crystallography*.²³ This material was chosen because of its technological relevance and its availability in large single-crystal form. There is one unique axis b that has two-fold rotational symmetry and a reflection plane perpendicular to the b -axis. (Either of these symmetry operations will result in the b -axis being a principal axis of the dielectric tensor.) The a - c plane is a cleavage plane, but the angle between the a - and c -axes is not normal but rather 91.5° .²³ Therefore, the direction of the reciprocal-space b^* -axis is parallel to the unique real-space b -axis, but the

reciprocal-space a^* and c^* directions are not aligned with the a - and c -axes, with deviations by 1.5° (see Fig. 1).

The CdWO₄ crystal is transparent, it is not hygroscopic, and the band gap is estimated to be 3.8–4.1 eV.²⁴ Prior to the ellipsometric measurements, three sides were polished using a Syton polish to reduce the surface roughness, while one of the remaining sides remained as-cut as a reference. A mark was placed on the as-cut surface indicating the b^* plane. The sample was nearly cubic with all face angles at $90^\circ \pm 0.4^\circ$. Four-circle x-ray measurements were performed to determine the crystallographic axes with respect to the sample faces.

There can often be confusion with respect to axis labeling, and there are different conventions among various communities. In this paper, we will use the right-handed coordinate system (x, y, z) to refer to the laboratory reference frame and (c, a, b) to refer to the axes of the crystal, described previously (see Fig. 1). The laboratory frame has z perpendicular to the sample surface pointing up, x in the plane of incidence, and y perpendicular to the plane of incidence. The faces of the sample cube are labeled (C, A, B). As determined from x-ray diffraction measurements, the crystallographic unique b -axis is perpendicular to the B face of the sample cube. The x-ray measurements showed that the a - and c -axes are mutually perpendicular to the unique b -axis, but the angle between the a - and c -axes is 91.5° . This is in agreement with previous

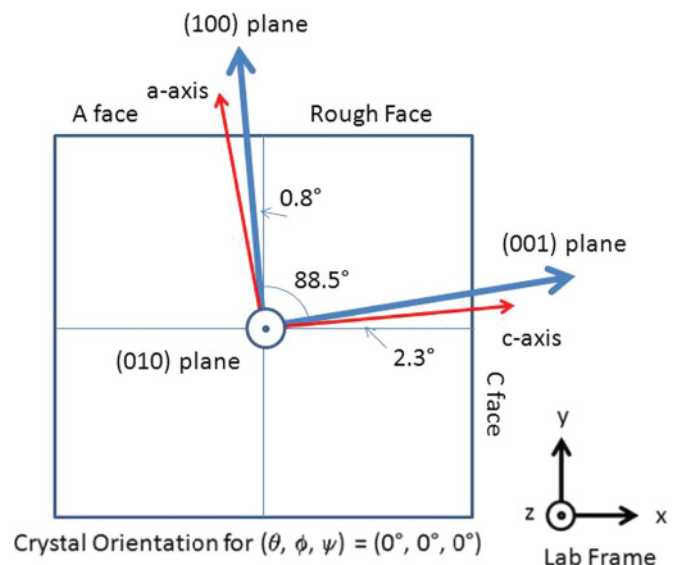


FIG. 1. (Color online) Schematic diagram relating the actual sample cube with the coordinate system of the crystal. The unique b -axis is perpendicular to the plane, out of the drawing. The a - and c -axes are denoted by the red arrows, while the (001) plane is perpendicular to the a - and b -axes, and the (100) plane is perpendicular to the b - and c -axes. The angle between the (100) and (001) planes is 88.5° , making the angle between the a - and c -axes 91.5° . The (100) plane is off the normal of the A face by 0.8° , and the (001) plane is off the normal of the C face by 2.3° . Similarly, the a -axis is off the normal of the A face by 2.3° , and the c -axis is off the normal of the C face by 0.8° . The sample cube as drawn is in the laboratory reference frame with the Euler angles $(\theta, \phi, \psi) = (0^\circ, 0^\circ, 0^\circ)$, where the z -axis is perpendicular to the plane of the page, the x -axis perpendicular to the C face and the y -axis perpendicular to the A face. The angles are not drawn to scale.

x-ray measurements.²³ The A face is 2.3° off the a -axis and 0.8° off the (100) plane. The C face is 0.8° off the c -axis and 2.3° off the (001) plane (see Fig. 1).

The initial values of the complex dielectric function as described in Eq. (1) are aligned with the sample cube. That is, ε_{33} corresponds to the dielectric function for light polarized parallel to the principal axis (the b -axis), perpendicular to the B face, while the quantities ε_{11} and ε_{22} correspond to the dielectric function for light polarized perpendicular to the C and A faces, respectively.

For an arbitrarily oriented monoclinic crystal with the dielectric tensor given in Eq. (1), one must apply an orthogonal coordinate transformation,

$$\varepsilon_{\text{lab}} = \mathbf{A}(\theta, \phi, \psi) \varepsilon_o \mathbf{A}^T(\theta, \phi, \psi), \quad (2a)$$

to rotate the crystal from its present position to the laboratory coordinate system. The transformation matrix \mathbf{A} uses the Euler angles θ , ϕ , and ψ ,²⁵ and is given by

$$\mathbf{A} = \begin{bmatrix} C_\phi C_\psi - C_\theta S_\phi S_\psi & S_\phi C_\psi + C_\theta C_\phi S_\psi & S_\theta S_\psi \\ -C_\phi S_\psi - C_\theta S_\phi C_\psi & -S_\phi S_\psi + C_\theta C_\phi C_\psi & S_\theta C_\psi \\ S_\theta S_\phi & -S_\theta C_\phi & C_\theta \end{bmatrix}, \quad (2b)$$

where we use the short-hand notation $C_\theta = \cos(\theta)$, $S_\theta = \sin(\theta)$, etc.

B. Reflection 2-MGE measurements

Generalized ellipsometry measurements were performed using the two-modulator generalized ellipsometer (2-MGE)^{26,27} at an angle of incidence of 64.84° . Twelve measurements were made, four measurements on each of the polished A, B, and C faces, with the sample rotated about the z -axis in the laboratory reference frame by 45° for each of the four measurements. For each of the faces measured, the accuracy of the Euler angle ψ for the initial alignment of the crystal cube on the sample stage was $\sim 0.5^\circ$, while the error in ψ for subsequent positions of the crystal was $\sim 0.2^\circ$. The configuration identity and Euler angles of rotation are shown in Table I. The letter associated with the configuration name

corresponds to the face that was used for the ellipsometric measurements, while the numbers refer to the Euler angle ψ .

The 2-MGE measures eight parameters simultaneously at each wavelength. If the polarization state generator (PSG) and the polarization state analyzer (PSA) are oriented at angles that are modulo 45° with respect to the plane of incidence, then the eight parameters correspond to eight elements of the normalized Mueller matrix (that is, $\mathbf{M}_{s,11}$ is set to 1).²⁶ Two zones were measured for this experiment, where the angles of the PSG and PSA were set to $(0^\circ, 45^\circ)$ for zone 1 and $(45^\circ, 0^\circ)$ for zone 2. Thus, all the off-block-diagonal elements of the sample Mueller matrix were measured at least one time (see Ref. 26 for the details). The accuracy of the 2-MGE data is typically 0.001–0.002 for parameters that range from -1 to $+1$, and it includes both systematic and random components. The accuracy does decrease in the ultraviolet (UV) range due to reduced light levels from the xenon lamp and in the near infrared due to the reduced sensitivity of the photomultiplier tube.

The elements of the sample Mueller matrix are then converted to the NSC representation, as described in Ref. 26. For isotropic samples, the NSC representation is directly related to the traditional ψ Δ and ρ representation of ellipsometry by

$$\rho = \frac{r_{pp}}{r_{ss}} = \tan(\psi) e^{i\Delta} = \frac{C + iS}{1 + N}. \quad (3a)$$

The NSC parameters are directly related to the elements of the sample Mueller matrix \mathbf{M}_s , where $N = -\mathbf{M}_{s,12} = -\mathbf{M}_{s,21}$, $S = \mathbf{M}_{s,34} = -\mathbf{M}_{s,43}$ components, and $C = \mathbf{M}_{s,33} = \mathbf{M}_{s,44}$. For anisotropic samples, cross polarization can occur, and this requires that four additional parameters become nonzero in any of the representations. These are given by:

$$\rho_{sp} = \frac{r_{sp}}{r_{ss}} = \tan(\psi_{sp}) e^{i\Delta_{sp}} = \frac{C_{sp} + iS_{sp}}{1 + N}, \quad (3b)$$

$$\rho_{ps} = \frac{r_{ps}}{r_{ss}} = \tan(\psi_{ps}) e^{i\Delta_{ps}} = \frac{C_{ps} + iS_{ps}}{1 + N}. \quad (3c)$$

The complex reflection coefficients are given by $r_{ij} = E_j^o / E_i^i$, where E_j^o (E_i^i) is the output (input) complex electric field projected parallel (p) or perpendicular (s) to the plane of

TABLE I. A summary of the configurations used in this study including the Euler angles. The column labeled (ϕ_1, ψ_1) gives the Euler angles used for the measurements, while the column labeled (ϕ_2, ψ_2) shows Euler angles that result in the same spectra. The fitted surface roughness and goodness of fit (χ^2) are also listed. The angle given for the B configurations is $\phi + \psi$.

Config. name	Euler angles ($^\circ$)			Rough	
	θ	(ϕ_1, ψ_1)	(ϕ_2, ψ_2)	d (nm)	χ^2
B000	0	0	180	4.38	0.94
B045	0	45	-135	4.29	0.96
B090	0	90	-90	4.21	1.22
B135	0	135	-45	4.23	1.11
C090	90	(-90, 90)	(90, 90)	2.88	0.62
C135	90	(-90, 135)	(90, 135)	2.83	0.72
C000	90	(-90, 180)	($\pm 90, 0$); (90, 180)	2.68	0.86
Cm135	90	(-90, -135)	(90, -135)	2.65	0.49
A000	90	(0, 180)	(0, 0); (0, 180); (180, 180)	3.39	0.96
Am135	90	(0, -135)	(180, -135)	3.32	0.74
Am90	90	(0, -90)	(180, -90)	3.31	0.55
Am45	90	(0, -45)	(180, -45)	3.20	0.53

incidence. The angles ψ and Δ are the traditional ellipsometric parameters (note that ψ here is the ellipsometric parameter and not the Euler angle). The cross-polarization terms are determined from the off-block-diagonal elements of the sample Mueller matrix, as described in Ref. 26.

The degree of polarization is given by:

$$\beta^2 = N^2 + S^2 + C^2 + S_{sp}^2 + C_{sp}^2 + S_{ps}^2 + C_{ps}^2. \quad (3d)$$

If $\beta = 1$, then no depolarization occurs, and $\beta < 1$ indicates that some depolarization has occurred. There is some residual depolarization in these measurements above ~ 5.4 eV

(< 230 nm), and $\beta = 0.92$ at 220 nm. To correct for this small amount of depolarization, the NSC parameters are first normalized using the β factor ($N_m = N/\beta$, etc.) before the ρ parameters are determined.

Note that we use the cross-polarization convention found in Azzam and Bashara²⁸ rather than that of Schubert.^{29,30} The primary reason is that symmetries in the cross-polarization terms that are obvious in the former representation are hidden in the latter representation.

Figure 2 shows representative generalized ellipsometry data for four different orientations of the sample, as described in

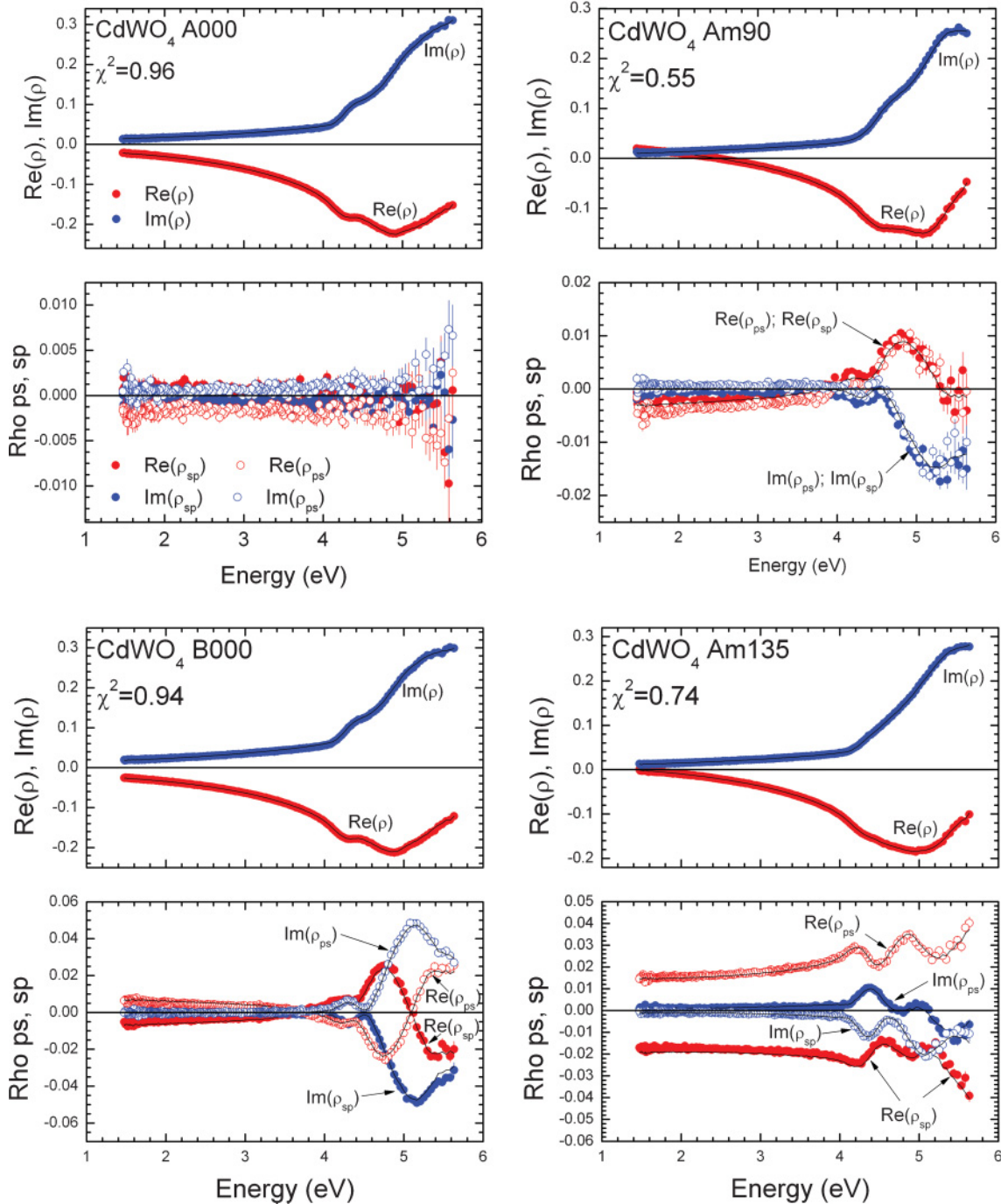


FIG. 2. (Color online) The real and imaginary parts of the complex reflection ratios for four different orientations of the sample, described in Table I. The thin lines show the fit to the data, described in the text, and the resulting χ^2 is also shown.

Table I. The thin black lines show the fit to the data using a procedure described later herein. As can be seen from the figures, the typical errors in ρ are 0.001–0.002. (This error estimate does not include the possible errors from the orientation of the crystal cube as reflected in the error in the Euler angle ψ .) Secondly, in all but a few cases (A000 and C000), the cross-polarization terms are nonzero at nearly all wavelengths. In some cases, obvious symmetry is observed, such as B000 in Fig. 2, while in other cases, such as Cm90 and Am135 in Fig. 2, the symmetry is lost, particularly above 4.0 eV. Furthermore, the ellipsometry data from several different orientations of the crystal show definite relationships one with another, which will be discussed later in the paper.

III. DATA ANALYSIS

The calculation of the complex reflection ratios shown in Eq. (2) for anisotropic materials is considerably more complicated than for isotropic materials, since cross polarization becomes nonzero in general. The procedure used for this paper is outlined in Refs. 31 and 32, but it basically follows the theory of Berreman²¹ as modified by Lin-Chung and Teitler,³³ Lin-Chung,³⁴ and Ong.³⁵ There are strong similarities with the formalism discussed by Schubert.^{29,30}

The Berreman equation is given by

$$\frac{d\Psi}{dz} = i\Delta\Psi, \quad (4)$$

where $\Psi = (E_x, H_y, E_y, -H_x)^T$ (not to be confused with the ellipsometric parameter ψ or the Euler angle ψ), and Δ is the complex Berreman matrix (not to be confused with the ellipsometric parameter Δ). For materials that are not optically active or magnetic, the Berreman matrix reduces to

$$\Delta = \begin{bmatrix} \Delta_{11} & \Delta_{12} & \Delta_{13} & 0 \\ \Delta_{21} & \Delta_{11} & \Delta_{23} & 0 \\ 0 & 0 & 0 & 1 \\ \Delta_{23} & \Delta_{13} & \Delta_{43} & 0 \end{bmatrix}. \quad (5a)$$

The elements of the Berreman matrix are

$$\Delta_{11} = -\xi \varepsilon_{13} / \varepsilon_{33}, \quad (5b)$$

$$\Delta_{12} = (\varepsilon_{33} - \xi^2) / \varepsilon_{33}, \quad (5c)$$

$$\Delta_{21} = \varepsilon_{11} - \varepsilon_{13}^2 / \varepsilon_{33}, \quad (5d)$$

$$\Delta_{13} = -\xi \varepsilon_{23} / \varepsilon_{33}, \quad (5e)$$

$$\Delta_{23} = \varepsilon_{12} - \varepsilon_{13} \varepsilon_{23} / \varepsilon_{33}, \quad (5f)$$

$$\Delta_{43} = \varepsilon_{22} - \xi^2 - \varepsilon_{23}^2 / \varepsilon_{33}, \quad (5g)$$

where $\xi = \sin(\varphi)$, and φ is the angle of incidence. The Berreman matrix of Eq. (5a) is not Hermitian, so its eigenvalues can be complex, and its eigenvectors are not orthogonal. The form of the Berreman matrix is different in Refs. 29 and 30, where a different vector Ψ is used. The two representations of the Berreman matrix are related by an orthogonal permutation transformation, so the eigenvalues and eigenvectors are unchanged.

A three-medium model was used for the near-surface region: air/surface roughness/bulk. The surface roughness was modeled using the Bruggeman effective medium model,³⁶ consisting of 50% voids and 50% material, where the isotropic dielectric function was the average of the three diagonal

components of the dielectric tensor. While this is clearly an approximation of the optical functions of the overlayer, the validity of the approximation is supported by the fitting procedure discussed below, where the goodness-of-fit parameter indicated a good fit. This is primarily because the overlayer thickness is thin, and the resulting dielectric functions are quite similar. A more accurate model of the surface overlayer would include the directionally dependent values of the dielectric tensor and would be necessary for a more anisotropic material.

The 4×4 transfer matrix χ_s for the material is the column-wise set of eigenvectors for the Δ matrix associated with the oriented bulk.^{31–34} The eigenvalues of the Δ matrix are first determined by solving the fourth-order secular equation. (This can be done analytically using Ferrari's method.) Once the eigenvalues λ_i are found, then the eigenvectors are given by

$$\mathbf{V} = \begin{bmatrix} V_1 \\ V_2 \\ V_3 \\ V_4 \end{bmatrix} = A \begin{bmatrix} \Delta_{11}\Delta_{13} - \Delta_{12}\Delta_{23} - \lambda\Delta_{13} \\ \Delta_{11}\Delta_{23} - \Delta_{21}\Delta_{13} - \lambda\Delta_{23} \\ -(\Delta_{11}^2 - \Delta_{21}\Delta_{12} - 2\lambda\Delta_{11} + \lambda^2) \\ -\lambda(\Delta_{11}^2 - \Delta_{21}\Delta_{12} - 2\lambda\Delta_{11} + \lambda^2) \end{bmatrix}. \quad (6)$$

Once these four eigenvectors are calculated, the two eigenvectors associated with the backward-propagating waves must be selected. These correspond to the two eigenvalues with negative imaginary parts. If the eigenvalues are real, then the positive eigenvalues are selected. The two eigenvectors associated with these eigenvalues are placed in the first and third columns of the χ_s matrix, where the first column contains the eigenvector where $(V_1V_1^* + V_2V_2^*) > (V_3V_3^* + V_4V_4^*)$ and the third column contains the eigenvector where $(V_1V_1^* + V_2V_2^*) < (V_3V_3^* + V_4V_4^*)$.

Note that the procedure discussed here is not valid for isotropic materials or anisotropic materials in certain symmetries that lead to cross-polarization coefficients that are zero. For isotropic materials, the equivalent Berreman transfer matrix consists of the 2×2 Abeles matrix for p -polarized light in the upper left block and the 2×2 Abeles for s -polarized light in the lower right block, where the off-block diagonal elements are zero.³⁵

The final characteristic matrix for the configuration considered here is given by:

$$\mathbf{M} = \chi_o \chi_f \chi_s. \quad (7)$$

The matrix χ_o is the characteristic matrix for the ambient, assuming that the ambient refractive index is 1:

$$\chi_o = \begin{bmatrix} 1 & \cos(\varphi) & 0 & 0 \\ -1 & \cos(\varphi) & 0 & 0 \\ 0 & 0 & \cos(\varphi) & 1 \\ 0 & 0 & \cos(\varphi) & -1 \end{bmatrix}. \quad (8)$$

Similarly, χ_f is the characteristic matrix for the film, given by:

$$\chi_f = \begin{bmatrix} \cos(\zeta) & i^* \sin(\zeta)^* \eta / \tilde{n} & 0 & 0 \\ i^* \sin(\zeta)^* \tilde{n} / \eta & \cos(\zeta) & 0 & 0 \\ 0 & 0 & \cos(\zeta) & i^* \sin(\zeta) / (\tilde{n}^* \eta) \\ 0 & 0 & i^* \sin(\zeta)^* \tilde{n}^* \eta & \cos(\zeta) \end{bmatrix}, \quad (9)$$

where $\zeta = 2\pi d \tilde{n} \eta / \lambda$, $\eta = \cos(\varphi_f)$, d is the thickness of the film, \tilde{n} is the complex refractive index, φ_f is the angle of incidence inside the film (possibly complex), and λ is the wavelength of light. The complex reflection ratios are calculated from the elements of the \mathbf{M} matrix:

$$r_{pp} = \frac{M_{23}M_{31} - M_{21}M_{33}}{M_{13}M_{31} - M_{11}M_{33}}, \quad (10a)$$

$$r_{ps} = \frac{M_{43}M_{31} - M_{41}M_{33}}{M_{13}M_{31} - M_{11}M_{33}}, \quad (10b)$$

$$r_{sp} = \frac{M_{21}M_{13} - M_{23}M_{11}}{M_{13}M_{31} - M_{11}M_{33}}, \quad (10c)$$

$$r_{ss} = \frac{M_{41}M_{13} - M_{43}M_{11}}{M_{13}M_{31} - M_{11}M_{33}}. \quad (10d)$$

The initial value of the surface roughness thickness for all the sample configurations was calculated using a Levenberg-Marquardt fit of the data below the band edge of the material (350 to 850 nm), using the Bruggeman effective medium approximation (50% voids, 50% bulk) for the film and the Sellmeier approximation for the bulk.³¹ These thicknesses, as well as the Euler angles given in Table I were then used to determine the initial values of the complex dielectric tensor for CdWO₄ by performing a point-by-point Levenberg-Marquardt fit on all 12 data sets. Since there are only eight independent values of the dielectric tensor, and there are $12 \times 6 = 72$ experimental data points at each wavelength, the system is significantly overdetermined. As a further refinement, the spectroscopic dielectric tensor components for CdWO₄ were then used in a fit to redetermine the surface roughness for each of the 12 measurements, and the spectroscopic dielectric tensor elements for monoclinic CdWO₄ were redetermined. A final fit of the individual spectra using the new spectroscopic dielectric tensor was performed, with the resulting χ^2 and surface roughness values shown in Table I for each of the 12 orientations. This determines the complex dielectric tensor for the sample cube in the ABC coordinate system, which is shown in Fig. 3.

IV. DISCUSSION

A. Dielectric Function

From Fig. 3, it can be seen that the monoclinic crystal CdWO₄ has four distinct complex values of the dielectric tensor at each wavelength. Below the band edge, the imaginary parts of the dielectric functions are 0, since the material is transparent in this region. The complex quantity ϵ_{33} corresponds to light polarized along the unique b -axis, which is the principal axis of the monoclinic crystal. The quantities ϵ_{11} and ϵ_{22} are not associated with fundamental axes in the crystal, but rather with the pseudocubic directions perpendicular to

the C and A faces, respectively, which are close to the c - and a -axes of the crystal. Although the angle between the a - and c -axes is nearly normal (91.5°), the unit cell still possesses only monoclinic symmetry. Naively, one might expect that the optical properties would be very close to an orthorhombic crystal, where the ϵ_{12} component of the dielectric tensor would be close to zero. However, the optical properties of the monoclinic crystal are determined by the symmetry of the unit cell, not the angles of the axes. As can be seen from Figs. 3 and 4, the ϵ_{12} component is significantly different from zero, and the monoclinic symmetry of the crystal structure has a distinctive optical signature. One consequence of this is that only the ϵ_{33} is definitively specified. The quantities ϵ_{11} , ϵ_{22} , and ϵ_{12} are given here with the a - and c -axes nearly aligned along the 22 and 11 directions, respectively. If a different coordinate system were defined using a rotation about the b -axis, then different quantities ϵ_{11} , ϵ_{22} , and ϵ_{12} would be obtained. Given the quantities ϵ_{11} , ϵ_{22} , and ϵ_{12} defined here,

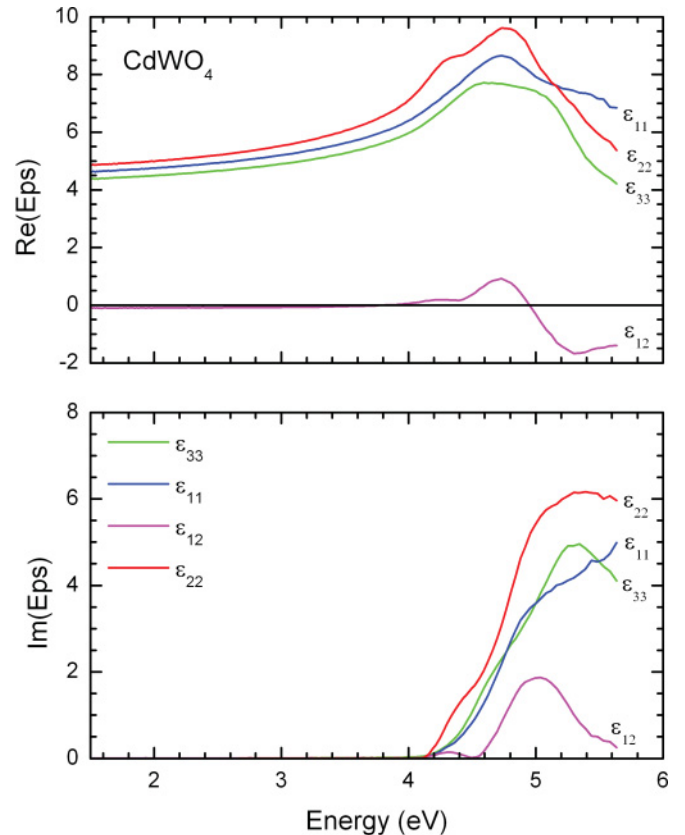


FIG. 3. (Color online) The complex dielectric tensor for CdWO₄. The values of the real part of ϵ_{12} are small but not 0. Figure 4 shows this data on an expanded scale.

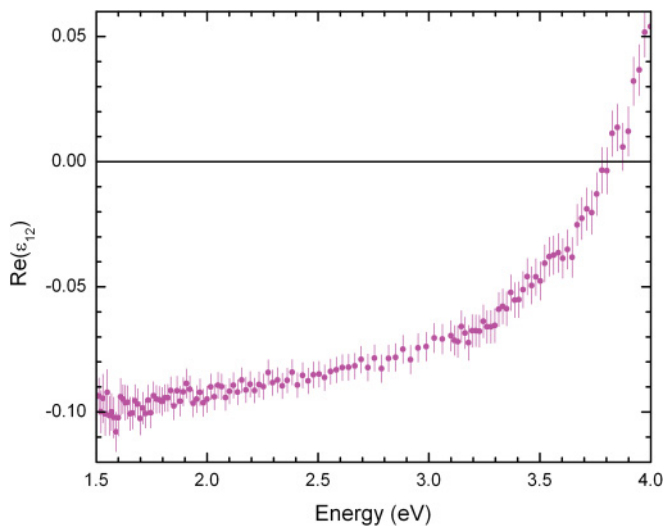


FIG. 4. (Color online) The real part of the off-diagonal element of the dielectric tensor below the band edge. This is expanded from the equivalent data shown in Fig. 3.

the new values would be simply those resulting from the Euler angle transformation of Eq. (2).

The values of the principal dielectric functions shown in Fig. 3 below the direct band edge obey the two-term Sellmeier approximation:

$$\varepsilon_{ii} = 1 + \frac{A_1 \lambda^2}{\lambda^2 - \lambda_{1o}^2} + \frac{A_2 \lambda^2}{\lambda^2 - \lambda_{2o}^2}, \quad (11)$$

with the fitting parameters shown in Table II. It will be noted that the reduced χ^2 is used as the figure of merit and is well below 1, indicating that the fit is good.

While it is not possible to diagonalize the dielectric tensor of a monoclinic crystal in general, it is possible to diagonalize the real and imaginary parts separately. Figure 5 shows the direction of the fast axis as a function of photon energy for the real and imaginary parts of the dielectric tensor, where the direction perpendicular to the C face is the reference axis. Note that the fast axis is the polarization direction of the smallest refractive index (real part) or smallest extinction coefficient (imaginary part) for light traveling along the unique *b*-axis of the crystal. As can be seen, the direction of the fast axis is a function of energy, and the directions of the fast axis for the real and imaginary parts are significantly different one from the other. The sign change in the fast axis for the real part near

TABLE II. The Sellmeier coefficients resulting from fits to the real part of the dielectric functions shown in Fig. 3 using Eq. (11). The fit was performed from 320 to 850 nm (3.88 to 1.46 eV). The goodness of fit parameter is the reduced χ^2 , indicating a good fit to the data (a good fit occurs when $\chi^2 < \sim 1$).

	ε_{11}	ε_{22}	ε_{33}
A_1	2.842	2.697	2.860
λ_{1o} (nm)	135.2	118.5	144.1
A_2	0.643	1.000	0.387
λ_{2o} (nm)	251.1	250.8	260.5
χ^2	0.16	0.14	0.18

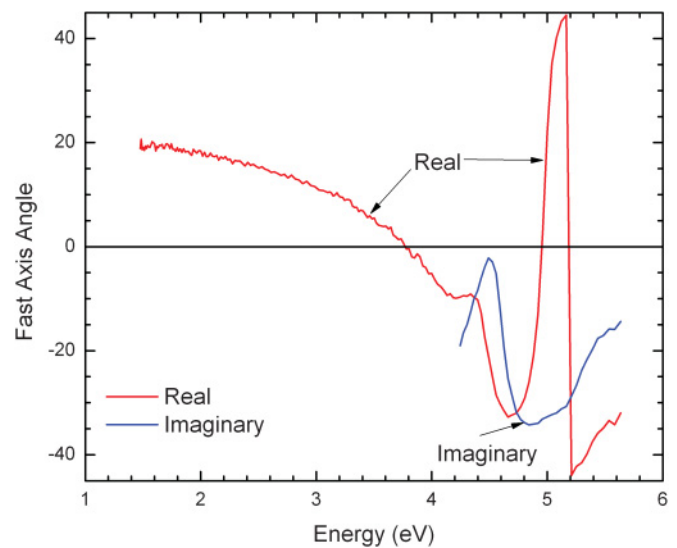


FIG. 5. (Color online) The direction of the fast axis as a function of photon energy for the real and imaginary parts. The light is passing along the *b*-axis, and the *c*-axis is the reference axis.

5.2 eV occurs because the sign of the real part of $\varepsilon_{22} - \varepsilon_{11}$ changes at that energy.

Below ~ 4 eV, CdWO₄ is transparent, so the imaginary part of the dielectric tensor vanishes, and it is possible to determine a unique principal axis system at each energy as shown in Fig. 5. Although the dielectric tensor is diagonalizable in the transparent region and the crystal is optically orthorhombic, the direction of the dielectric function axes perpendicular to the unique *b*-axis is a function of energy. The direction of the fast axis crosses zero (the C face normal) near 3.8 eV (i.e., 326 nm), corresponding to $\varepsilon_{12} = 0$, within error. Moreover, at this energy, both the real and imaginary parts of ρ_{ps} and ρ_{sp} of the data sets where the projected principal axes are in the plane of incidence or perpendicular to the plane of incidence (B000, B090, A000, Am90, C000, C090) are also zero within error. This can be seen in Fig. 2 for data sets A000, B000, and Am90, respectively. The other data sets are not shown, but they behave in a similar manner. Therefore, at this wavelength, the monoclinic CdWO₄ crystal is optically orthorhombic with the principal axes aligned with the laboratory coordinate system. This is very similar to the case of ZnO, where the normally uniaxial ZnO crystal is optically isotropic at 292 nm (i.e., 4.25 eV).^{11,37}

It has been suggested by Schmidt *et al.*^{17–19} that one can apply a projection operator to the dielectric tensor to reduce the four complex elements of the dielectric tensor to three complex elements of a polarization matrix. To examine this, we have applied this projection operator on the dielectric function tensor data shown in Fig. 3, varying the Euler angle ϕ and projection angle γ to minimize the off-diagonal elements in the polarization matrix, where the details are shown in Appendix A. The results show that this model works well on the data of Fig. 3 in the transparent region of the crystal, but it does not work well if the entire measured spectrum is included. Thus, four spectroscopic complex values of the dielectric tensor are required to describe monoclinic crystals. This is totally in accord with the theoretical understanding of the dielectric functions.^{1–3}

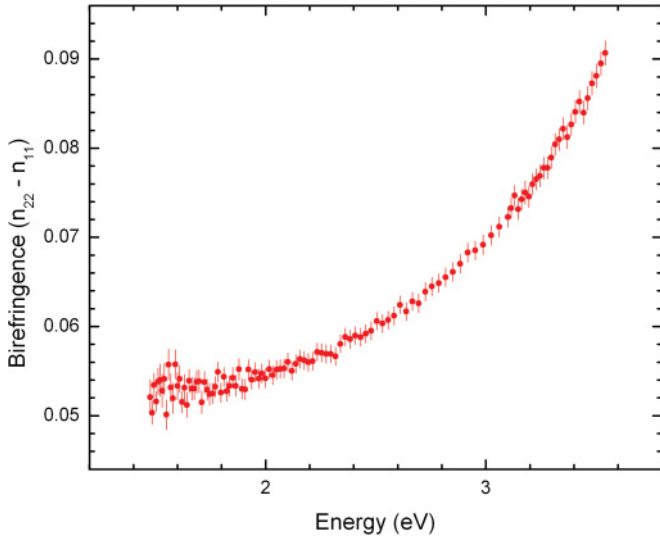


FIG. 6. (Color online) The birefringence of CdWO_4 in the transparent region for light passing parallel to the b -axis.

Another feature of a monoclinic crystal is that it behaves as a retarder for light passing along the b -axis. However, as discussed above, the direction of the fast axis changes with wavelength. Figure 6 shows the birefringence of the crystal for light passing along the unique b -axis.

B. Symmetry in the complex reflection ratios ρ

As can be seen from Fig. 2, the complex Fresnel reflection ratios ρ , ρ_{sp} , and ρ_{ps} show quite a complicated behavior as a function of crystal orientation, but there also is a considerable amount of apparent symmetry in the data. The observed symmetries are summarized in Table III.

For ellipsometric measurements on the B face of the crystal, the principal axis is perpendicular to the sample surface. This corresponds to the measured configurations B000, B045, B090, and B135, where the Euler angle $\theta = 0^\circ$. The Euler angles ϕ and ψ are degenerate, so we can set $\psi = 0^\circ$ without loss of generality. In this set of configurations, we observe that $\rho_{ps} = -\rho_{sp}$ for any orientation of ϕ (see Fig. 2, B000). That is, one can rotate the Euler ϕ angle to any value, and this relation will hold. If two ellipsometric spectra are taken with orientations of ϕ and $\phi + 90^\circ$, then the magnitudes of the cross-polarization terms appear to be the same, but they will change sign. However, the magnitude of the ρ_{pp} term

will depend on ϕ . Any rotation of the crystal by 180° will leave the ellipsometric response unchanged, as required by the 2-fold rotational symmetry of the crystal.

If the b -axis is perpendicular to the plane of incidence (Euler angles $\theta = 90^\circ, \psi = 0^\circ, 180^\circ, \phi$ variable, configurations A000 and C000), then the cross-polarization terms are 0, regardless of the angle ϕ (see Fig. 2, A000). However, the ρ_{pp} term does depend upon ϕ and still shows the 180° rotational symmetry about the b -axis, so $\rho_{pp}(\phi) = \rho_{pp}(\phi + 180^\circ)$.

If the b -axis is parallel to the plane of incidence and in the sample surface plane (Euler angles $\theta = 90^\circ, \psi = \pm 90^\circ, \phi$ variable, configurations Am090 and C090), then the cross-polarization terms are equal, but not equal to zero (see Fig. 2, Am90). That is, $\rho_{sp}(\phi) = \rho_{ps}(\phi) \neq 0$ and will depend upon the angle ϕ . The ρ_{pp} term will also vary with ϕ but will give the same values when ϕ is rotated by 180° . From Table I, it can be seen that experimental configurations Am90 and C090 correspond to equivalent Euler angles and should, therefore, yield identical spectra. Within experimental error, this is the case.

Other configurations (Am135, Am45, C135, and Cm135) show no symmetry within the data for that particular orientation (see Fig. 2, Am135), but they do show apparent symmetry when compared with ellipsometric data taken in other orientations. For example, the data for the Am135 orientation shows no correlation between ρ_{ps} and ρ_{sp} . However, comparing the data of Cm135 with C135, one finds that $\rho_{sp}(\text{Cm135}) \cong \rho_{ps}(\text{C135})$, $\rho_{ps}(\text{Cm135}) \cong \rho_{sp}(\text{C135})$, and $\rho_{pp}(\text{Cm135}) \cong \rho_{pp}(\text{C135})$. Another similar finding can be applied to the Am45 and Am135 pair of ellipsometric data. Here, the rotation of the crystal changes the sign of the cross-polarization terms but leaves the ρ_{pp} term unchanged. That is, $\rho_{ps}(\text{Am45}) \cong -\rho_{ps}(\text{Am135})$, $\rho_{sp}(\text{Am45}) \cong -\rho_{sp}(\text{Am135})$, and $\rho_{pp}(\text{Am45}) \cong \rho_{pp}(\text{Am135})$.

To understand these observed symmetries, we need to transform the dielectric tensor into the laboratory reference frame, calculate the Berreman matrix, determine the eigenvalues and eigenvectors, calculate the transfer matrix and the characteristic matrix of the system, and then calculate the complex reflection coefficients. This process was outlined previously herein and is applied to three symmetry directions in Appendices B–D.

When the b -axis is perpendicular to the plane of incidence, then the dielectric tensor takes the form of Eq. (1). As the crystal is rotated about the b -axis (Euler angle rotation ϕ), the

TABLE III. The observed symmetries in the complex reflection ratios from monoclinic crystals for various orientations of the unique b -axis. The B face is perpendicular to the b -axis.

Axis orientation	Symmetries
b \perp SS	$\rho_{ps}(\phi) = -\rho_{sp}(\phi)$ $\rho(\phi) = \rho(\phi + 180^\circ)$ for pp , sp , and ps $\rho_{ps}(\phi) \cong -\rho_{ps}(\phi + 90^\circ); \rho_{sp}(\phi) \cong -\rho_{sp}(\phi + 90^\circ)$, but $\rho_{pp}(\phi) \neq \rho_{pp}(\phi + 90^\circ)$
b \perp POI; \parallel SS	$\rho_{sp}(\phi) = \rho_{ps}(\phi) = 0$
b \parallel POI; \parallel SS	$\rho_{ps}(\phi) = \rho_{sp}(\phi) \neq 0$

SS = sample surface. POI = plane of incidence.

tensor values will change (except for the ϵ_{33} term), but the tensor will remain symmetric, and the 0 elements will remain zero (see Appendix B). From the calculations in Appendix B [Eq. (B9a)], we obtain:

$$\rho_{ps} = -\rho_{sp} = \frac{2\eta_o \Delta_{12} \Delta_{23}(\phi)}{F_{ss}(\phi)}, \quad (12)$$

where $\eta_o = \cos(\phi)$, ϕ is the angle of incidence, Δ_{12} and $\Delta_{23}(\phi)$ are elements of the Berreman matrix [see Eq. (5)], and $F_{ss}(\phi)$ is a complicated factor containing the dielectric functions and the angles. If ϕ is rotated by 90° , then Δ_{12} remains the same, but $\Delta_{23}(\phi)$ changes sign, and $F_{ss}(\phi)$ will also change. For many cases, $F_{ss}(\phi)$ is much larger than the numerator and will not change significantly with ϕ , resulting in the pseudosymmetry shown in Table II. A rotation of 180° of a monoclinic crystal will result in the same dielectric tensor, so the ellipsometric response will be unchanged.

The observation that $\rho_{ps} = -\rho_{sp}$ for b perpendicular to the sample surface can also be explained using the argument of Li,³⁸ who invoked the reciprocity theorem of conical grating diffraction of Vincent and Neviere.³⁹ References 38 and 39 were applied specifically to diffraction gratings, but the only required symmetry feature that was invoked was the 2-fold rotational symmetry about the surface normal. Since a monoclinic crystal with the principal axis perpendicular to the sample surface has the same symmetry, then the same relationship holds.

If the b -axis is perpendicular to the plane of incidence, then it is observed that the cross-polarization terms are zero. From the calculation described in Appendix C, this comes about because the Berreman matrix is block-diagonal, giving rise to a block-diagonal set of eigenvectors, which will naturally lead to cross-polarization terms that are zero. Another way of looking at the situation is that if the principal axis is perpendicular to the plane of incidence, then the other two axes will have to be in the plane of incidence. Therefore, the plane of incidence determines the symmetry of the ellipsometric experiment (as for isotropic media), there is no mixing of the s -polarized state with the p -polarized state, and no cross polarization should result.

If the b -axis is in the plane of incidence, parallel to the sample surface, then cross polarization is observed, but $\rho_{ps} = \rho_{sp}$ for all angles ϕ . This is shown in Appendix D.

V. CONCLUSIONS

We have shown that generalized ellipsometry spectra taken on 12 orientations of a monoclinic crystal can be used to determine the complex dielectric tensor of the material. For a given orientation of the crystal, the dielectric tensor is symmetric with four independent complex quantities. Although x-ray measurements show that the a - and c -axes are nearly orthogonal, the off-diagonal element ϵ_{12} is significantly different from zero, particularly above the band gap at ~ 4 eV. Moreover, the energy dependence of both the real and imaginary parts of ϵ_{12} bears no relation to the other components of the dielectric tensor. Below the band edge, it is possible to uniquely diagonalize the dielectric tensor, but the fast-axis angle will now depend on energy. Above the band edge, it is not possible to uniquely diagonalize the dielectric

tensor. The nonorthogonal transformation of Suh *et al.*²⁰ as employed by Schmidt *et al.*^{17–19} cannot be used to describe this monoclinic crystal.

The raw ellipsometric spectra show various symmetries in the complex reflection ratios ρ , depending on the orientation of the principal symmetry b -axis. If the b -axis is perpendicular to the sample surface, then the cross-polarization terms ρ_{sp} and ρ_{ps} will be equal in magnitude but opposite in sign, and their magnitudes will depend upon the orientation of the crystal as represented by the Euler angle ϕ . That is: $\rho_{ps}(\phi) = -\rho_{sp}(\phi)$. If the b -axis is perpendicular to the plane of incidence, then both the cross-polarization terms go to: $\rho_{sp}(\phi) = \rho_{ps}(\phi) = 0$. This is because the a - and c -axes now lie in the plane of incidence, and there is no mixing of the s - and p -polarization states. If the b -axis is in the plane of incidence, parallel to the sample surface, then the cross-polarization terms are equal but generally unequal to zero. That is: $\rho_{ps}(\phi) = \rho_{sp}(\phi)$.

ACKNOWLEDGMENTS

This research has been supported by the Laboratory Directed Research and Development (LDRD) program of Oak Ridge National Laboratory (ORNL) and by the NA-22/NNSA program of the Department of Energy. Research at the Oak Ridge National Laboratory for G.E.J., L.A.B., J.D.B., and E.D.S. is sponsored in part by the US Department of Energy, Basic Energy Sciences, Materials Sciences and Engineering Division. ORNL is managed by UT-Battelle, LLC, for the US Department of Energy.

APPENDIX A: COMPARISON WITH THE PROJECTION OPERATOR FORMALISM OF SCHMIDT *ET AL.* (REFS. 17–19)

In Refs. 17–19, Schmidt *et al.* propose a nonorthogonal transformation to reduce the dielectric tensor containing four complex values at each wavelength to a diagonal complex matrix. The expression used for this transformation is given by

$$\epsilon = R^T(TPT^T - I)R, \quad (A1a)$$

TABLE IV. The best-fit results of the projection operator transformation shown in Eq. (A2) using the complex dielectric function data shown in Fig. 3. Column A shows the resultant χ^2 when no projection occurs from the projection operator. Columns B through E show the fitted values of ϕ and γ and the resultant χ^2 for four different values of (ϕ, γ) resulting in local minima in χ^2 . Columns C and E are symmetry replicas of columns B and D resulting from the symmetry operation $\phi \rightarrow \phi + 180^\circ$.

	A	B	C	D	E
Transparent region					
Euler ϕ ($^\circ$)	0	25.6	205.6	115.6	295.6
Tilt angle γ ($^\circ$)	90	92.2	92.2	87.7	87.7
χ^2	181.5	0.33	0.32	0.92	0.92
Full spectrum					
Euler ϕ ($^\circ$)	0	34.9	214.9	124.9	304.9
Tilt angle γ ($^\circ$)	90	92.4	92.4	87.6	87.6
χ^2	428.8	40.32	40.32	48.73	48.83

where R is the rotation matrix

$$R = \begin{bmatrix} \cos(\phi) & -\sin(\phi) & 0 \\ \sin(\phi) & \cos(\phi) & 0 \\ 0 & 0 & 1 \end{bmatrix}, \quad (\text{A1b})$$

and T is the nonorthogonal transformation, given by

$$T = \begin{bmatrix} 1 & \cos(\gamma) & 0 \\ 0 & \sin(\gamma) & 0 \\ 0 & 0 & 1 \end{bmatrix}. \quad (\text{A1c})$$

The dielectric function tensor is given in Eq. (1), the quasipolarization matrix P (normally notated as ρ in Refs. 17–19) is given by

$$P = \begin{bmatrix} P_{11} & P_{12} & 0 \\ P_{21} & P_{22} & 0 \\ 0 & 0 & P_{33} \end{bmatrix}, \quad (\text{A1d})$$

and I is the identity matrix.

Equation (A1a) can be inverted using pre- and postmultiplication by appropriate matrices to give

$$P = T^{-1}(R\epsilon R^T - I)(T^T)^{-1}. \quad (\text{A2})$$

The matrix T is not orthogonal, but it is also nonsingular, so it does possess an inverse. However, the inverse is not the transpose, as it would be for an orthogonal transformation matrix. Using this expression, it can be shown that the P matrix is symmetric, so $P_{12} = P_{21}$. If this transformation is valid, then it must be possible to find angles γ and ϕ , where the complex off-diagonal element P_{12} is 0 over the entire wavelength range, where we are to use the CdWO₄ data shown in Fig. 3 for the spectroscopic values of the dielectric tensor ϵ . The figure of merit used for this calculation is the reduced χ^2 :

$$\chi^2 = \frac{1}{2N} \sum_{k=0}^N \left[\frac{\text{Re}(P_{12}(\lambda_k))^2}{\text{Re}(\delta P_{12}(\lambda_k))^2} + \frac{\text{Im}(P_{12}(\lambda_k))^2}{\text{Im}(\delta P_{12}(\lambda_k))^2} \right], \quad (\text{A3})$$

where N is the number of wavelength points, $\text{Re}(P_{12})$ and $\text{Im}(P_{12})$ are the real and imaginary parts of the off-diagonal matrix element P_{12} , and $\text{Re}(\delta P_{12})$ and $\text{Im}(\delta P_{12})$ are the real and imaginary parts of the propagated errors from the errors of the measured elements of the complex dielectric function tensor ϵ . If the lowest values of the reduced χ^2 are < 1 , then the model fits the data including errors. The best-fit values of the angles γ and ϕ were found by a combination of Monte Carlo analysis used for a global search over $-90^\circ < \gamma < 90^\circ$ and $0 \leq \phi < 360^\circ$ and a Levenberg-Marquardt algorithm to polish the fit, reducing the reduced χ^2 to its local minimum.

The results of the calculation are shown in Table IV, where column A shows the results if no projection operator is used. In the transparent region of the crystal (1.5–4.0 eV), where

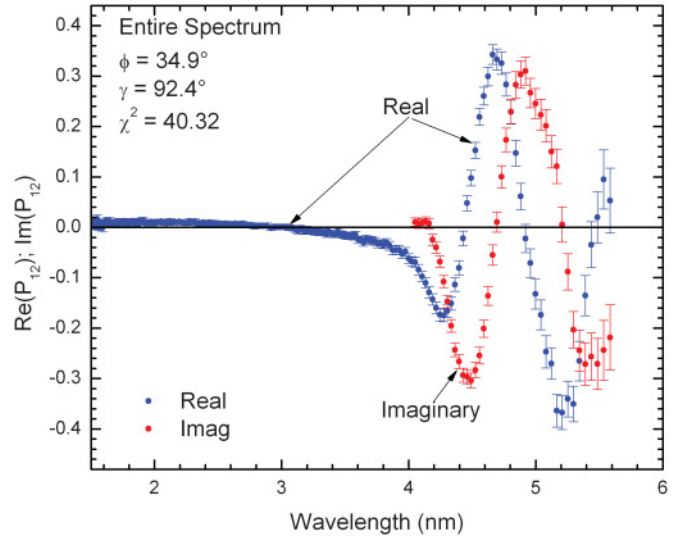


FIG. 7. (Color online) The spectroscopic real and imaginary parts of the off-diagonal element of the polarization matrix P_{12} .

the complex dielectric tensor is real, four values of (γ, ϕ) can be found where $\chi^2 < 1$, indicating that the projection operator model does fit the data. For this calculation, $\text{Im}(P_{12})$ is set to 0, and the prefactor in Eq. (A3) is $1/N$ rather than $1/(2N)$. From symmetry, if one solution is found for (γ, ϕ) , then a complementary solution must also be found for $(\gamma, \phi + 180^\circ)$. In addition, nearly complementary solutions must be found at $(180^\circ - \gamma, \phi + 90^\circ)$ and $(180^\circ - \gamma, \phi - 90^\circ)$. This is the case with the data shown in Table IV.

The bottom of Table IV shows the results if the entire spectrum is included in the fit. As with the results limited to the transparent region, there are four solutions related by symmetry. However, the resulting reduced χ^2 values for the entire spectrum for all four solutions are > 40 , indicating that the projection operator model does not fit the values of the complex dielectric tensor shown in Fig. 3. The spectroscopic values of the real and imaginary parts of P_{12} are shown in Fig. 7 using the values of γ and ϕ for which the χ^2 was a minimum.

APPENDIX B. PRINCIPAL AXIS PERPENDICULAR TO THE SAMPLE SURFACE: B FACE

To determine the dielectric tensor in the laboratory reference frame, the monoclinic dielectric tensor in Eq. (1) is rotated using the Euler transformation shown in Eq. (2). For the case where the unique b -axis is perpendicular to the sample surface, $\theta = 0^\circ$, the effective angle is $\phi + \psi$, so ψ can be set to 0° with no loss of generality. The dielectric tensor in the laboratory reference frame takes the form

$$\epsilon_{\text{lab}} = \begin{bmatrix} \epsilon_{11}C_\phi^2 + 2\epsilon_{12}C_\phi S_\phi + \epsilon_{22}S_\phi^2 & \epsilon_{12}(C_\phi^2 - S_\phi^2) + C_\phi S_\phi(\epsilon_{22} - \epsilon_{11}) & 0 \\ \epsilon_{12}(C_\phi^2 - S_\phi^2) + C_\phi S_\phi(\epsilon_{22} - \epsilon_{11}) & \epsilon_{22}C_\phi^2 - 2\epsilon_{12}C_\phi S_\phi + \epsilon_{11}S_\phi^2 & 0 \\ 0 & 0 & \epsilon_{33} \end{bmatrix}. \quad (\text{B1})$$

Applying this to the Berreman matrix [Eq. (5)], we find that $\Delta_{11} = \Delta_{13} = 0$ and

$$\begin{aligned}\Delta_{23}(\phi) &= \varepsilon_{12}(C_\phi^2 - S_\phi^2) + C_\phi S_\phi(\varepsilon_{22} - \varepsilon_{11}) \\ &= \varepsilon_{12}C_{2\phi} + \frac{S_{2\phi}}{2}(\varepsilon_{22} - \varepsilon_{11}),\end{aligned}\quad (\text{B2a})$$

$$\Delta_{12} = 1 - \xi^2/\varepsilon_{33}; \quad (\text{B2b})$$

$$\Delta_{21}(\phi) = \varepsilon_{11,\text{lab}}; \quad (\text{B2c})$$

$$\Delta_{43}(\phi) = \varepsilon_{22,\text{lab}} - \xi^2. \quad (\text{B2d})$$

Therefore, $\Delta_{23}(\phi) = \Delta_{23}(\phi + 180^\circ) = -\Delta_{23}(\phi \pm 90^\circ)$. The Berreman matrix element Δ_{12} is independent of ϕ , but Δ_{21} and Δ_{43} are functions of ϕ . Rotations about the unique b -axis by 180° will result in the same dielectric tensor and the same Berreman matrix and, therefore, the same ellipsometric response. The resulting Berreman matrix will be:

$$\Delta = \begin{bmatrix} 0 & \Delta_{12} & 0 & 0 \\ \Delta_{21}(\phi) & 0 & \Delta_{23}(\phi) & 0 \\ 0 & 0 & 0 & 1 \\ \Delta_{23}(\phi) & 0 & \Delta_{43}(\phi) & 0 \end{bmatrix}. \quad (\text{B3})$$

We use the secular equation to determine the eigenvalues λ

$$\begin{aligned} & \begin{vmatrix} -\lambda & \Delta_{12} & 0 & 0 \\ \Delta_{21}(\phi) & -\lambda & \Delta_{23}(\phi) & 0 \\ 0 & 0 & -\lambda & 1 \\ \Delta_{23}(\phi) & 0 & \Delta_{43}(\phi) & -\lambda \end{vmatrix} \\ &= \lambda^4 - \lambda^2 [\Delta_{43}(\phi) + \Delta_{12}\Delta_{21}(\phi)] \\ & \quad + \Delta_{12} [\Delta_{21}(\phi)\Delta_{43}(\phi) - \Delta_{23}^2(\phi)] = 0. \end{aligned} \quad (\text{B4})$$

Note that the secular equation has only even powers of λ , and the Δ_{23} term enters only to second order. Using the quadratic formula to solve Eq. (B4) yields

$$\begin{aligned} \lambda^2 &= \frac{1}{2} [\Delta_{43}(\phi) + \Delta_{12}\Delta_{21}(\phi) \\ & \quad \pm \sqrt{(\Delta_{12}\Delta_{21}(\phi) - \Delta_{43}(\phi))^2 + 4\Delta_{12}\Delta_{23}(\phi)^2}]. \end{aligned} \quad (\text{B5})$$

From Eq. (6), the four eigenvectors of the Berreman matrix will be of the form

$$\mathbf{V} = \begin{bmatrix} V_1 \\ V_2 \\ V_3 \\ V_4 \end{bmatrix} = A \begin{bmatrix} -\Delta_{12}\Delta_{23}(\phi) \\ -\lambda\Delta_{23}(\phi) \\ -\lambda^2 + \Delta_{21}(\phi)\Delta_{12} \\ -\lambda(\lambda^2 - \Delta_{21}(\phi)\Delta_{12}) \end{bmatrix}. \quad (\text{B6})$$

Two of the eigenvalues will correspond to the positive sign in Eq. (B5), which we label λ_p , and two will correspond to the

negative sign, which we label λ_n . The characteristic matrix for the bulk becomes

$$\chi_s = \begin{bmatrix} -\Delta_{12}\Delta_{23}(\phi) & 0 & -\Delta_{12}\Delta_{23}(\phi) & 0 \\ -\lambda_p\Delta_{23}(\phi) & 0 & -\lambda_n\Delta_{23}(\phi) & 0 \\ \lambda_p^2 - \Delta_{21}(\phi)\Delta_{12} & 0 & \lambda_n^2 - \Delta_{21}(\phi)\Delta_{12} & 0 \\ \lambda_p(\lambda_p^2 - \Delta_{21}(\phi)\Delta_{12}) & 0 & \lambda_n(\lambda_n^2 - \Delta_{21}(\phi)\Delta_{12}) & 0 \end{bmatrix}. \quad (\text{B7})$$

If the film is ignored, then the total characteristic matrix $\mathbf{M} = \chi_o\chi_s$. From Eq. (10), the complex reflection ratios are given by

$$r_{ps} = -\frac{2\eta_o\Delta_{12}\Delta_{23}(\phi)^2(\lambda_p - \lambda_n)}{\text{Denom}}, \quad (\text{B8a})$$

$$r_{sp} = \frac{2\eta_o\Delta_{12}\Delta_{23}(\phi)^2(\lambda_p - \lambda_n)}{\text{Denom}}, \quad (\text{B8b})$$

$$r_{pp} = -\frac{\Delta_{23}(\phi)(\lambda_p - \lambda_n)F_{pp}(\phi)}{\text{Denom}}, \quad (\text{B8c})$$

$$r_{ss} = -\frac{\Delta_{23}(\phi)(\lambda_p - \lambda_n)F_{ss}(\phi)}{\text{Denom}}. \quad (\text{B8d})$$

The eigenvalues λ_p and λ_n are for the forward-propagating waves, and the terms F_{pp} and F_{ss} are complicated terms containing the eigenvalues λ_p and λ_n , η_o , and all the matrix elements of the Berreman matrix. From the definition of the reflection coefficient ratios in Eq. (3), we get:

$$\rho_{ps} = -\rho_{sp} = \frac{2\eta_o\Delta_{12}\Delta_{23}(\phi)}{F_{ss}(\phi)}, \quad (\text{B9a})$$

where

$$\begin{aligned} F_{ss}(\phi) &= \Delta_{12}[\Delta_{43} - \eta_o^2\Delta_{21} - \eta_o(\lambda_n + \lambda_p) + \lambda_n\lambda_p] \\ & \quad + \lambda_n\lambda_p\eta_o(\lambda_n + \lambda_p - \eta_o). \end{aligned} \quad (\text{B9b})$$

Therefore, the magnitudes of the ρ_{ps} and ρ_{sp} reflection ratios are equal, but they differ by their signs. From Eq. (B2a), a 90° rotation of ϕ switches the sign of $\Delta_{23}(\phi)$, but $F_{ss}(\phi) \neq F_{ss}(\phi + 90^\circ)$, resulting in $\rho_{sp}(\phi) \cong -\rho_{sp}(\phi + 90^\circ)$, $\rho_{ps}(\phi) \cong -\rho_{ps}(\phi + 90^\circ)$. A rotation of 180° leaves ρ_{ps} and ρ_{sp} invariant.

APPENDIX C: PRINCIPAL AXIS PERPENDICULAR TO THE PLANE OF INCIDENCE

If the b -axis is perpendicular to the plane of incidence, then the eigenvalues and eigenvectors of the Berreman matrix are simplified considerably. This case was measured using the two configurations A000 and C000. Both configurations require the Euler angle θ to be 90° , the ψ angle set to 0° or 180° , and ϕ is free. For this orientation of the crystal, the dielectric tensor in the laboratory reference frame is given by:

$$\varepsilon_{\text{lab}} = \begin{bmatrix} \varepsilon_{11}C_\phi^2 + 2\varepsilon_{12}C_\phi S_\phi + \varepsilon_{22}S_\phi^2 & 0 & -b[\varepsilon_{12}(C_\phi^2 - S_\phi^2) + C_\phi S_\phi(\varepsilon_{22} - \varepsilon_{11})] \\ 0 & \varepsilon_{33} & 0 \\ -b[\varepsilon_{12}(C_\phi^2 - S_\phi^2) + C_\phi S_\phi(\varepsilon_{22} - \varepsilon_{11})] & 0 & \varepsilon_{22}C_\phi^2 - 2\varepsilon_{12}C_\phi S_\phi + \varepsilon_{11}S_\phi^2 \end{bmatrix}, \quad (\text{C1})$$

where $b = \cos(\psi) = \pm 1$.

The Berreman matrix elements $\Delta_{13} = \Delta_{23} = 0$, and

$$\Delta_{11}(\phi) = \xi b \frac{\varepsilon_{12} C_{2\phi} + \frac{S_{2\phi}}{2} (\varepsilon_{22} - \varepsilon_{11})}{\varepsilon_{22} C_{\phi}^2 - 2\varepsilon_{12} C_{\phi} S_{\phi} + \varepsilon_{11} S_{\phi}^2}, \quad (\text{C2a})$$

$$\Delta_{12}(\phi) = 1 - \xi^2 / \varepsilon_{33, \text{lab}}(\phi); \quad (\text{C2b})$$

$$\Delta_{21}(\phi) = \varepsilon_{11, \text{lab}}(\phi) - \varepsilon_{13, \text{lab}}(\phi)^2 / \varepsilon_{33, \text{lab}}(\phi), \quad (\text{C2c})$$

$$\Delta_{43} = \varepsilon_{22, \text{lab}} - \xi^2. \quad (\text{C2d})$$

That is, Δ_{43} is independent of ϕ , while the other Berreman matrix elements depend on ϕ . The resulting Berreman matrix is:

$$\Delta = \begin{bmatrix} \Delta_{11}(\phi) & \Delta_{12}(\phi) & 0 & 0 \\ \Delta_{21}(\phi) & \Delta_{11}(\phi) & 0 & 0 \\ 0 & 0 & 0 & 1 \\ 0 & 0 & \Delta_{43}(\phi) & 0 \end{bmatrix}. \quad (\text{C3})$$

Since the Berreman matrix Δ in Eq. (C3) is block-diagonal, the eigenvalues and eigenvectors are simple. The four eigenvalues

$$\varepsilon_{\text{lab}} = \begin{bmatrix} \varepsilon_{33} & 0 & 0 & 0 \\ 0 & \varepsilon_{11} C_{\phi}^2 + 2\varepsilon_{12} C_{\phi} S_{\phi} + \varepsilon_{22} S_{\phi}^2 & b[\varepsilon_{12}(C_{\phi}^2 - S_{\phi}^2) + C_{\phi} S_{\phi}(\varepsilon_{22} - \varepsilon_{11})] & 0 \\ 0 & b[\varepsilon_{12}(C_{\phi}^2 - S_{\phi}^2) + C_{\phi} S_{\phi}(\varepsilon_{22} - \varepsilon_{11})] & \varepsilon_{22} C_{\phi}^2 - 2\varepsilon_{12} C_{\phi} S_{\phi} + \varepsilon_{11} S_{\phi}^2 & 0 \end{bmatrix}. \quad (\text{D1})$$

The Berreman matrix elements $\Delta_{11} = \Delta_{23} = 0$ and

$$\Delta_{13}(\phi) = \xi b \frac{\varepsilon_{12} C_{2\phi} + \frac{S_{2\phi}}{2} (\varepsilon_{22} - \varepsilon_{11})}{\varepsilon_{22} C_{\phi}^2 - 2\varepsilon_{12} C_{\phi} S_{\phi} + \varepsilon_{11} S_{\phi}^2}, \quad (\text{D2a})$$

$$\Delta_{12}(\phi) = 1 - \xi^2 / \varepsilon_{33, \text{lab}}; \quad (\text{D2b})$$

$$\Delta_{21} = \varepsilon_{11, \text{lab}}; \quad (\text{D2c})$$

$$\Delta_{43}(\phi) = \varepsilon_{22, \text{lab}} - \xi^2 - \varepsilon_{23, \text{lab}}^2 / \varepsilon_{33, \text{lab}}. \quad (\text{D2d})$$

The quantity $b = \sin(\psi) = \pm 1$. The Berreman matrix element Δ_{21} is independent of ϕ , while the other elements are dependent on ϕ . The resulting Berreman matrix becomes:

$$\Delta = \begin{bmatrix} 0 & \Delta_{12}(\phi) & \Delta_{13}(\phi) & 0 \\ \Delta_{21} & 0 & 0 & 0 \\ 0 & 0 & 0 & 1 \\ 0 & \Delta_{13}(\phi) & \Delta_{43}(\phi) & 0 \end{bmatrix}. \quad (\text{D3})$$

are just (Δ_{43} , $-\Delta_{43}$, $b\Delta_{11} + \sqrt{[\Delta_{12}\Delta_{21}]}$, $b\Delta_{11} + \sqrt{[\Delta_{12}\Delta_{21}]}$), and the ordered eigenvectors give the transfer matrix

$$\chi_s = \begin{bmatrix} \sqrt{\frac{\Delta_{12}(\phi)}{\Delta_{21}(\phi)}} & -\sqrt{\frac{\Delta_{12}(\phi)}{\Delta_{21}(\phi)}} & 0 & 0 \\ 1 & 1 & 0 & 0 \\ 0 & 0 & \sqrt{\Delta_{43}} & -\sqrt{\Delta_{43}} \\ 0 & 0 & 1 & 1 \end{bmatrix}. \quad (\text{C4})$$

Since this transfer matrix is block-diagonal, then the cross-polarization reflection ratios ρ_{ps} and ρ_{sp} must be 0. This also holds true if there is a surface film, as long as the film is isotropic. Since this holds for any value of ϕ , then the cross-polarization terms are equal zero whenever the principal axis is perpendicular to the plane of incidence

APPENDIX D: PRINCIPAL AXIS IS PARALLEL TO THE PLANE OF INCIDENCE, PARALLEL TO THE SAMPLE SURFACE

If the Euler angle $\theta = 90^\circ$ and $\psi = \pm 90^\circ$, then the dielectric tensor in the laboratory reference frame simplifies to:

The secular equation is

$$\lambda^4 - \lambda^2[\Delta_{43}(\phi) + \Delta_{12}(\phi)\Delta_{21}] + \Delta_{21}[\Delta_{12}(\phi)\Delta_{43}(\phi) - \Delta_{13}(\phi)^2] = 0, \quad (\text{D4})$$

which is very similar to Eq. (B4), but Δ_{12} and Δ_{21} are interchanged, and Δ_{23} is replaced with Δ_{13} . Following the same procedure as in Appendix B, we obtain:

$$r_{ps} = r_{sp} = \frac{2\eta_o \Delta_{21} \Delta_{13}(\phi)}{F_{ss}(\phi)}, \quad (\text{D5a})$$

where

$$F_{ss}(\phi) = -\eta_o \Delta_{21} [\Delta_{43} - \Delta_{12} - \eta_o(\lambda_n + \lambda_p) + \lambda_n \lambda_p] - \lambda_n \lambda_p (\lambda_n + \lambda_p - \eta_o). \quad (\text{D5b})$$

Therefore, the cross-polarization terms are equal if the principal axis is parallel to the sample surface and in the plane of incidence. Rotations about ϕ will alter the magnitudes of ρ_{sp} and ρ_{ps} , but the relations Eq. (D5a) will hold.

*Corresponding author: jellisongejr@ornl.gov

¹G. N. Ramchandran and S. Ramaseshan, *Crystal Optics, in Handbuch der Physik*, edited by S. Fluegge (Springer, Berlin, 1961) Vol. 25/1, p. 1.

²M. Born, and E. Wolf, *Principles of Optics*, 6th edition (Cambridge University Press, Cambridge, 1993).

³R. W. Collins, and A. S. Ferlauto, in *Handbook of Ellipsometry*, edited by H. G. Tompkins and E. A. Irene, (William Andrew, Norwich, NY, 2005), Chap. 2.

⁴D. E. Aspnes and A. A. Studna, *Phys. Rev. B* **27**, 985 (1983).

⁵G. E. Jellison Jr., *Opt. Mat.* **1**, 41 (1992).

⁶G. E. Jellison Jr., I. Paulauskas, L. A. Boatner, and D. J. Singh, *Phys. Rev. B* **74**, 155130 (2006).

⁷J. Li, N. J. Podraza, and R. W. Collins, *Phys. Stat. Sol. A* **205**, 91 (2007).

⁸G. E. Jellison Jr., S. Auluck, D. J. Singh, and L. A. Boatner, *J. Appl. Phys.* **107**, 013514 (2010).

⁹T. E. Tiwald, and M. Schubert, *Proc. SPIE* **4103**, 19 (2000).

- ¹⁰G. E. Jellison Jr., L. A. Boatner, J. D. Budai, B. S. Jeong, and D. P. Norton, *J. Appl. Phys.* **93**, 9537 (2003).
- ¹¹G. E. Jellison Jr. and L. A. Boatner, *Phys. Rev. B* **58**, 3586 (1998).
- ¹²D. W. Thompson, M. J. DeVries, T. E. Tiwald, and J. A. Woollam, *Thin Sol. Films* **313-314**, 341 (1998).
- ¹³M. I. Alonso, M. Garriga, *Thin Solid Films* **455-456**, 124 (2004).
- ¹⁴M. I. Alonso, M. Garriga, N. Karl, J. O. Ossó, and F. Schriber, *Org. Electr.* **3**, 23 (2002).
- ¹⁵S. Tavazzi, and M. Campione, *Appl. Phys. Lett.* **88**, 071918 (2006).
- ¹⁶S. Tavazzi, S. Mora, L. Alessandrini, and L. Silverstri, *J. Chem. Phys.* **134**, 034707 (2011).
- ¹⁷D. Schmidt, A. C. Kjerstad, T. Hofmann, R. Skomski, E. Schubert, and M. Schubert, *J. Appl. Phys.* **105** 113508 (2009).
- ¹⁸D. Schmidt, B. Booso, T. Hofmann, E. Schubert, A. Sarangan, and M. Schubert, *Opt. Lett.* **34**, 992 (2009).
- ¹⁹D. Schmidt, B. Booso, T. Hofmann, E. Schubert, A. Sarangan, and M. Schubert, *Appl. Phys. Lett.* **94**, 011914 (2009).
- ²⁰I.-H. Suh, Y.-S. Park, and J.-G. Kim, *Appl. Crystallogr.* **33**, 994 (2000).
- ²¹D. W. Berreman, *J. Opt. Soc. Am.* **62**, 502, (1972).
- ²²M. Moszynski, M. Balcerzyk, M. Kapusta, A. Syntfeld, D. Wolski, G. Pausch, J. Stein, and P. Schotanus, *IEEE Trans. Nucl. Sci.* **52**, 3124 (2005).
- ²³M. Daturi, G. Busca, M. M. Borel, A. Leclaire, and P. Piaggio, *J. Phys. Chem. B* **101**, 4358 (1997).
- ²⁴Y. Abraham, N. A. W. Holtzwarth, and R. T. Williams, *Phys. Rev. B* **62**, 1733 (2001).
- ²⁵H. Goldstein, *Classical Mechanics* (Addison-Wesley, Cambridge, 1950).
- ²⁶G. E. Jellison Jr. and F. A. Modine, *Appl. Opt.* **36**, 8190 (1997).
- ²⁷G. E. Jellison Jr. and F. A. Modine, *Appl. Opt.* **36**, 8184 (1997).
- ²⁸R. M. A. Azzam, and N. M. Bashara, *Ellipsometry and Polarized Light* (North Holland, New York, 1977).
- ²⁹M. Schubert, *Phys. Rev. B* **53**, 4265 (1996).
- ³⁰M. Schubert, in *Handbook of Ellipsometry*, edited by H. G. Tompkins and E. A. Irene (William Andrew, Norwich, NY, 2005), Chap. 9.
- ³¹G. E. Jellison Jr., *Thin Sol. Films* **313-314**, 33 (1998).
- ³²G. E. Jellison Jr., in *Handbook of Ellipsometry*, edited by H. G. Tompkins and E. A. Irene (William Andrew, Norwich, NY, 2005), Chap. 3.
- ³³P. J. Lin-Chung and S. Teitler, *J. Opt. Soc. Am. A* **1**, 703 (1984).
- ³⁴P. J. Lin-Chung, *Superlatt. Microstruct.* **13**, 93 (1992).
- ³⁵H. L. Ong, *J. Opt. Soc. Am. A* **8**, 303 (1991).
- ³⁶D. A. G. Bruggeman, *Ann. Phys. (Leipzig)* **24**, 636 (1936).
- ³⁷G. E. Jellison Jr. and C. M. Rouleau, *Appl. Opt.* **44**, 3153 (2005).
- ³⁸L. Li, *J. Opt. Soc. Am. A* **17**, 881 (2000).
- ³⁹P. Vincent and M. Nevriere, *Opt. Acta* **26**, 889 (1979).